

All-angle negative refraction without negative effective index

Chiyan Luo, Steven G. Johnson, and J. D. Joannopoulos*

Department of Physics and Center for Materials Science and Engineering, Massachusetts Institute of Technology, Cambridge, Massachusetts 02139

J. B. Pendry

Condensed Matter Theory Group, The Blackett Laboratory, Imperial College, London SW7 2BZ, United Kingdom

(Received 22 January 2002; published 13 May 2002)

We describe an all-angle negative refraction effect that does not employ a negative effective index of refraction and involves photonic crystals. A few simple criteria sufficient to achieve this behavior are presented. To illustrate this phenomenon, a microsperlens is designed and numerically demonstrated.

DOI: 10.1103/PhysRevB.65.201104

PACS number(s): 78.20.Ci, 42.70.Qs, 42.30.Wb

Negative refraction of electromagnetic waves in “left-handed materials” has become of interest recently because it is the foundation for a variety of novel phenomena.^{1–6} In particular, it has been suggested that negative refraction leads to a superlensing effect that can potentially overcome the diffraction limit inherent in conventional lenses.² These phenomena have been described in the context of an effective-medium theory with negative index of refraction, and at the moment only appear possible in the microwave regime. To explore the possibility of negative refraction in the optical regime, one may turn to photonic crystals as interesting alternatives. Recent experimental⁷ and theoretical⁸ works indicate that negative refraction phenomena in photonic crystals are possible in regimes of negative group velocity and negative effective index above the first band near the Brillouin-zone center (Γ). However, lower frequencies in the band structure may be more desirable in high-resolution superlensing, as we discuss later in this paper. Here, we show that negative refraction can also be achieved without employing materials with negative effective index. In particular, our focus is on the *lowest* photonic band near a Brillouin-zone corner farthest from Γ . Interestingly, this band has a positive group velocity and a *positive* refractive index, but a negative photonic “effective mass.” We exhibit a frequency range so that for all incident angles one obtains only a single, negative-refracted beam. Such all-angle negative refraction (AANR) is essential for superlens applications.

Although our analysis is general, we study two dimensional (2D) photonic crystals for simplicity. We begin with TE modes (in-plane electric field) and consider a square lattice of air holes in dielectric $\epsilon=12.0$ (e.g., Si at $1.55\ \mu\text{m}$), with lattice constant a and hole radius $r=0.35a$. To visualize and analyze diffraction effects, we employ wave-vector diagrams: constant-frequency contours in \mathbf{k} space whose gradient vectors give the group velocities of the photonic modes. Our numerical calculations are carried out in a plane-wave basis by preconditioned conjugate-gradient minimization of the block Rayleigh quotient using a freely available software package developed in-house.⁹ A root finder is used to solve for the exact wave vectors that lead to a given frequency. The results for frequencies throughout the lowest photonic band are shown in Fig. 1.

We observe from Fig. 1 that due to the negative-definite photonic effective mass $\partial^2\omega/\partial k_i\partial k_j$ at the M point, the frequency contours are *convex* in the vicinity of M and have inward-pointing group velocities. For frequencies that correspond to all-convex contours, negative refraction occurs as illustrated in Fig. 2. The distinct refracted propagating modes are determined by the conservation of the frequency and the wave-vector component parallel to the air/photonic-crystal surface. If the surface normal is along ΓM [(11) direction], and the contour is everywhere *convex*, then an incoming plane wave from air will couple to a single mode that propagates into this crystal on the *negative* side of the boundary normal. We have thus realized negative refraction in the first band.

It is clear from this example that neither a negative group velocity nor a negative effective index is a prerequisite for negative refraction. In fact, the lowest band here has $\mathbf{k}\cdot\partial\omega/\partial\mathbf{k}\geq 0$ everywhere within the first Brillouin zone, meaning that the group velocity is never opposite to the phase velocity. In this sense, we are operating in a regime of *positive* effective index. In fact, our photonic crystal is behaving much like a *uniform*, “right-handed” medium with hyperbolic dispersion relations, such as those induced by an-

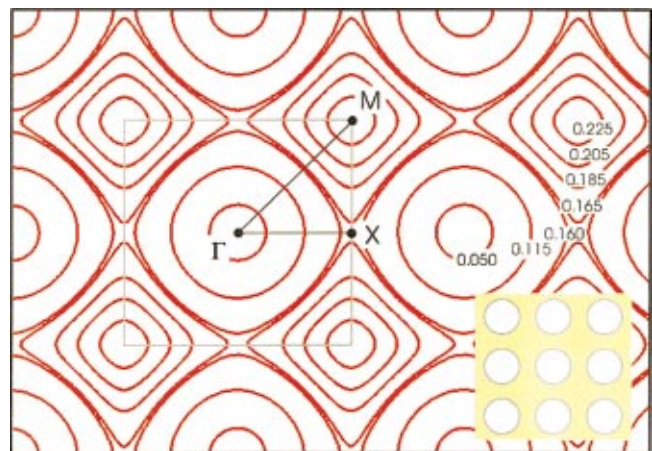


FIG. 1. (Color) Several constant-frequency contours of the first band of a model photonic crystal, drawn in the repeated zone scheme. Frequency values are in units of $2\pi c/a$.

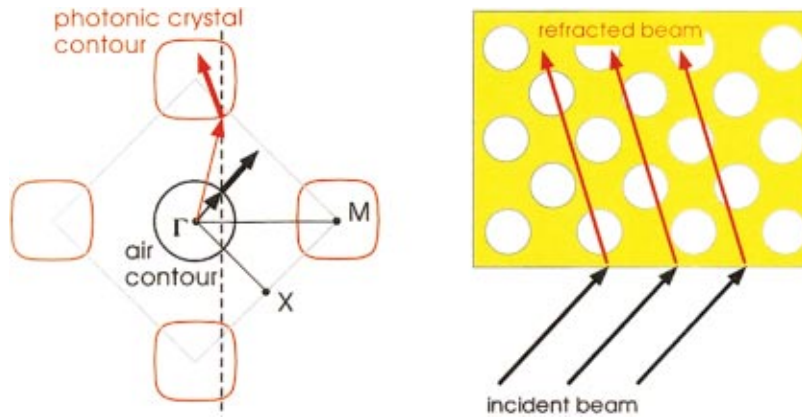


FIG. 2. (Color) Left panel: negative-refracted beams constructed from constant-frequency contours and conservation of surface-parallel wave vector. Thick arrows indicate group-velocity directions, and thin arrows stand for phase-velocity directions. Right panel: diagram of refracted rays in the actual crystal.

isotropy. For example, the TE modes in a nonmagnetic medium with dielectric tensor

$$\tilde{\epsilon} = \begin{pmatrix} \epsilon_1 & 0 \\ 0 & \epsilon_2 \end{pmatrix}$$

with $\epsilon_1 > 0$ and $\epsilon_2 < 0$ have a dispersion relation $k_2^2/\epsilon_1 - k_1^2/|\epsilon_2| = \omega^2/c^2$. Similar negative refraction will then happen on the (01) surface. Again, the phase velocity always makes an acute angle with the group velocity.

To realize AANR for superlensing, the required conditions in our model system are that the photonic-crystal contours be both *convex* and *larger* than the constant-frequency contours for air, i.e., circles with radius ω/c . Incident beams at *any* incident angle will then experience negative refraction when entering the photonic crystal. Note that single-beam behavior is only possible for $\omega \leq 0.5 \times 2\pi c/a_s$ (where a_s is the surface-parallel period) in order to avoid diffraction. Thus, there are three key criteria that are sufficient to guarantee single-beam AANR.

(i) The constant-frequency contour of the photonic crystal is all convex with a negative photonic effective mass.

(ii) All incoming wave vectors at such a frequency are included within the constant-frequency contour of the photonic crystal.

(iii) The frequency is below $0.5 \times 2\pi c/a_s$.

Using these criteria, we have calculated the AANR frequency range in our model system. We find two regions where AANR is possible, as shown in Fig. 3. These exist in the first and second bands, and correspond to positive and negative effective indices, respectively. The lower-frequency range has an upper limit $\omega_u = 0.198 \times 2\pi c/a$ that is obtained directly from the band structure by finding the intersection with the light line as depicted in Fig. 3. We find the lower limit to be $\omega_l = 0.186 \times 2\pi c/a$, by computing the frequency at which the radius of curvature of the contours along ΓM diverges. This leads to a fractional AANR frequency range of 6.1% around $0.192 \times 2\pi c/a$. For the second band, we obtain an AANR range of only 0.7% around $0.287 \times 2\pi c/a$.

To demonstrate how AANR can be put to use, we design a microsperlens using the same photonic crystal. Ideally, such a superlens can focus a point source on one side of the lens into a *real* point image on the other side even for the case of a parallel-sided slab of material.^{1,2} Such a superlens

possesses several key advantages over conventional lenses. Due to the lack of an optical axis, strict alignment is not necessary. Moreover, flat slabs instead of curved shapes are used and thus fabrication may be easier in principle. A superlens also operates over distances on the order of wavelengths and is an ideal candidate for small-scale integration. Furthermore, AANR for a superlens means that there is essentially no physical limit on the aperture of this imaging system. Finally, for superlensing at a given configuration and wavelength λ , the resolution of a superlens is expected to be limited by the surface period a_s , the characteristic length in our problem. Thus the frequency region of preference, yielding the potentially highest resolution, should correspond to the smallest a_s/λ . Since typically $a_s \sim a$ and $a/\lambda = \omega a/2\pi c$, this implies that we should choose to operate at the lowest AANR values of $\omega a/2\pi c$ in our band structure.

In order to model such a superlens, we have performed finite-difference time-domain (FDTD) simulations with perfectly matched layer boundary conditions¹⁰ on a parallel-sided (11)-oriented slab of our photonic crystal as shown in Fig. 4. Depicted here is a snapshot of the magnetic field for a continuous-wave (CW) point source placed at a distance $0.35a$ from the left-hand surface. The frequency is $0.195 \times 2\pi c/a$, chosen to lie within the lowest AANR frequency range. Note the formation of a “point” image on the right-hand side of the superlens at a distance of $0.38a$. Moreover,

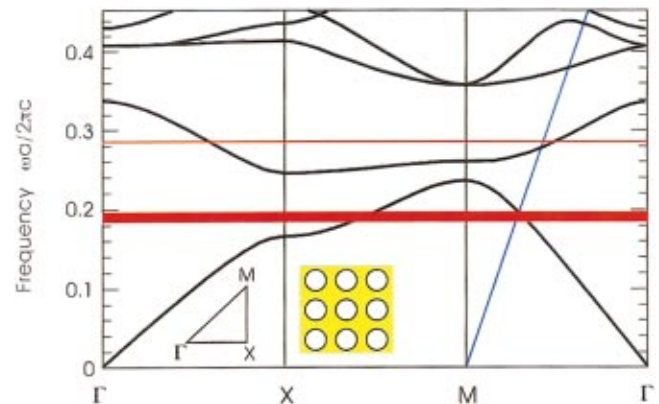


FIG. 3. (Color) The AANR frequency ranges are highlighted in red in the band structure. The light line shifted to M is shown in blue.

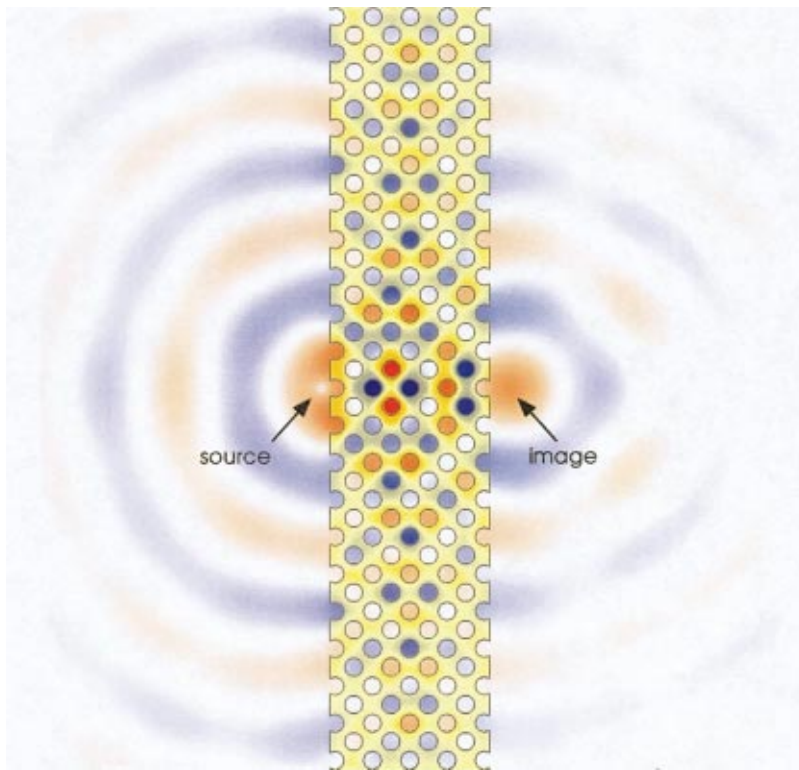


FIG. 4. (Color) H_z field of a point source and its image across a photonic-crystal superlens (yellow). Blue, white, and red correspond, respectively, to negative, zero, and positive H_z .

even though $a_s = \sqrt{2}a$ in this case, the frequency is low enough that we obtain a transverse size of only 0.67λ . Although small aberrations are visible in the field pattern, the simulation clearly demonstrates the superlensing effect of this photonic crystal. A similar calculation in the second band AANR region for a slab oriented along (10) with a_s

$=a$ also gives a focused image. Even though a_s/a is smaller now, the image turns out to have a larger transverse size 0.76λ , in accordance with our intuition that lower frequencies in the band structure offer better superlensing resolution. For both cases the thickness and surface termination of our slab in the simulation are chosen to minimize reflections.

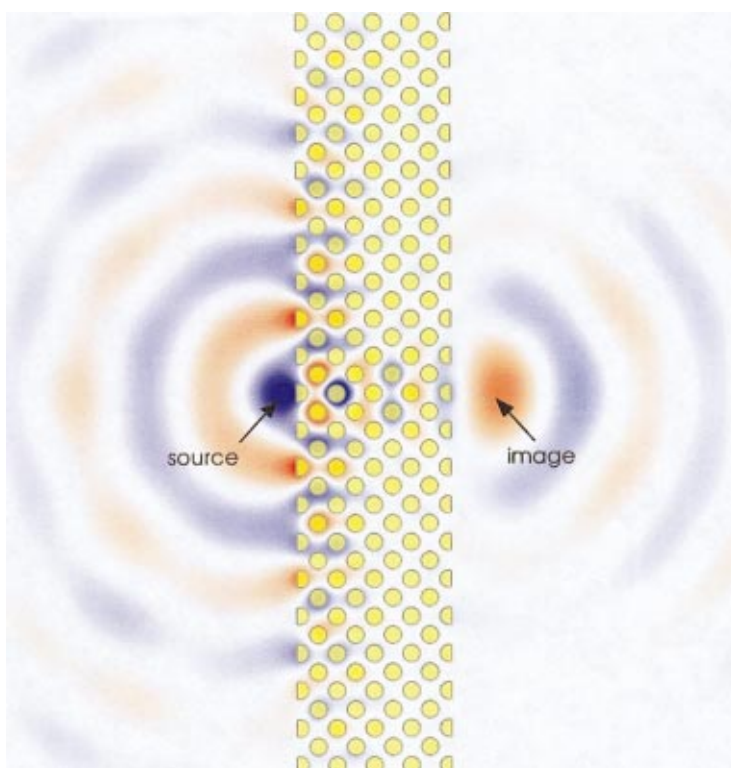


FIG. 5. (Color) E_z field of a point source and its image across a photonic-crystal superlens (yellow). Blue, white, and red correspond respectively to negative, zero, and positive E_z .

This is accomplished by requiring a slab to possess both mirror symmetry and a thickness equal to an integer multiple of half the wavelength in the slab. Normal-incident transmission through the slab then reaches a resonance maximum for the source frequency and stays above 99% for a range of incident angles of typically at least $\pm 40^\circ$. The slab thickness also determines the maximum object distance from the left-hand face that can lead to a good image at a given frequency: the ray-crossing point induced by negative refraction must lie *within* the superlens. In general, thicker slabs will be able to focus more distant objects.

The preceding discussion focused on the TE modes of a “holes-in-dielectric” structure. However, based on the general criteria presented here one can obtain single-beam AANR for TM modes (in-plane magnetic field) as well. For TM modes in a similar holes-in-dielectric system with $\epsilon = 12$, one can obtain a narrow AANR range of width 0.6% around $0.20 \times 2\pi c/a$ by increasing the hole radii to $r = 0.45a$. Alternatively, if a “rods-in-air” structure is used with dielectric-rod radii $r = 0.3a$ and the dielectric constant is increased to 14 (e.g., a mixture of glass spheres and alumina flake, at microwave length scales), the TM modes can have a larger AANR range of about 3.5% near $0.192 \times 2\pi c/a$. Further increasing the dielectric constant in this structure with the same rod radii to $\epsilon = 18$, e.g., that of Ge at $1.55 \mu\text{m}$, could widen the AANR frequency range to 5.2% around $0.172 \times 2\pi c/a$. We have performed FDTD simulations of

the rods-in-air structure with $\epsilon = 14$ and $r = 0.3a$, and the result is shown Fig. 5. The superlensing phenomenon is again clearly discernable. In this case, however, the reflectivity off the left-hand surface is somewhat higher than in Fig. 4, and there are stronger aberrations in the field pattern. Note that it also happens that here the source and the image are roughly π out of phase. In general arbitrary phase shifts are possible and can be chosen by design.

Although we have focused our analysis on 2D photonic crystals, it should be noted that such 2D-periodic crystals can be readily studied in 3D. For example, the experiments of McCall *et al.*¹¹ use a photonic-crystal slab sandwiched between two metal plates and exhibit 2D TM modes in the microwave regime. We conjecture that similar results might also be obtainable in the optical regime by replacing the metallic components with multilayer films with a large gap, or simply by index guiding.¹² Although true single-beam refraction is difficult to achieve in 3D, our ideas of AANR with positive effective index also generalize naturally to 3D-periodic crystals and could lead to realistic superlens applications.

This work was supported in part by the MRSEC program of the NSF under Grant No. DMR-9400334 and the DoD/ONR MURI Grant No. N00014-01-1-0803. C. L. acknowledges financial support from MIT.

*Electronic address: joannop@mit.edu

¹V. G. Veselago, Usp. Fiz. Nauk **92**, 517 (1964) [Sov. Phys. Usp. **10**, 509 (1968)].

²J. B. Pendry, Phys. Rev. Lett. **85**, 3966 (2000).

³J. B. Pendry, A. J. Holden, W. J. Stewart, and I. Youngs, Phys. Rev. Lett. **76**, 4773 (1996).

⁴J. B. Pendry, A. J. Holden, D. J. Robbins, and W. J. Stewart, IEEE Trans. Microwave Theory Tech. **47**, 2075 (1999).

⁵D. R. Smith, W. J. Padilla, D. C. View, S. C. Nemat-Nasser, and S. Schultz, Phys. Rev. Lett. **84**, 4184 (2000).

⁶R. A. Shelby, D. R. Smith, and S. Schultz, Science **292**, 77

(2001).

⁷H. Kosaka, T. Kawashima, A. Tomita, M. Notomi, T. Tamamura, T. Sato, and S. Kawakami, Phys. Rev. B **58**, 10 096 (1998).

⁸M. Notomi, Phys. Rev. B **62**, 10 696 (2000).

⁹S. G. Johnson and J. D. Joannopoulos, Opt. Express **8**, 173 (2001).

¹⁰J.-P. Berenger, J. Comput. Phys. **114**, 185 (1994).

¹¹S. L. McCall, P. M. Platzman, R. Dalichaouch, D. Smith, and S. Schultz, Phys. Rev. Lett. **67**, 2017 (1991).

¹²S. G. Johnson, S. Fan, P. R. Villeneuve, J. D. Joannopoulos, and L. A. Kolodziejski, Phys. Rev. B **60**, 5751 (1999).